Journal of Computational and Applied Mathematics 392 (2021) 113441

Contents lists available at ScienceDirect

Journal of Computational and Applied Mathematics

journal homepage: www.elsevier.com/locate/cam

A parallel multilevel domain decomposition method for source identification problems governed by elliptic equations

Xiaomao Deng [a,1], Zi-Ju Liao [b,1], Xiao-Chuan Cai [c,*]

[a] School of Mathematics and Statistics, Guangdong University of Foreign Studies, Guangzhou, Guangdong 510006, China
[b] Department of Mathematics, College of Information Science and Technology, Jinan University, Guangzhou, Guangdong 510632, China
[c] Department of Mathematics, University of Macau, Macau, China

ARTICLE INFO

Article history:
Received 12 December 2019
Received in revised form 3 August 2020

MSC:
65K10
65Y05
49M05
49M27

Keywords:
Domain decomposition
Parallel computing
Source identification
Inverse problems

ABSTRACT

In this paper we develop a parallel multilevel domain decomposition method for large-scale source identification problems governed by elliptic equations. A popular approach is to formulate the inverse problem as a PDE-constrained optimization problem. The minima satisfies a Karush–Kuhn–Tucker (KKT) system consisting of the state, adjoint and source equations which is rather difficult to solve on parallel computers. We propose and study a parallel method that decomposes the optimization problem on the global domain into subproblems on overlapping subdomains, each subdomain is further decomposed to form an additive Schwarz preconditioner for solving these smaller subproblems simultaneously with a preconditioned Krylov subspace method. For each subproblem, the overlapping part of the solution is discarded and the remaining non-overlapping part of the solution is put together to obtain an approximated global solution to the inverse problem. Since all the subproblems are solved independently, the multilevel domain decomposition method has the advantage of higher degree of parallelism. Numerical experiments show that the algorithm is accurate in terms of the reconstruction error and has reasonably good speedup in terms of the computing time. The efficiency and robustness of the proposed approach on a parallel computer with more than 1, 000 processors are reported.

1. Introduction

We consider the source identification problem governed by elliptic equations. The problem can be described as identifying the source function by using some given measurements of the solution of the elliptic problem. Such problems appear in many scientific and engineering applications such as identifying the source of electrostatic potential [1], the illegal wells in seawater intrusion phenomenon [2], the optical energy absorption distribution in photoacoustic tomography [3], etc. Several algorithms for source identification problems are available [4–10]. For example, in [7] using Green's function, the location and intensity of the point sources are reconstructed from scattered boundary measurements. In [9] an alternative iterative correction algorithm is introduced to compute the source in a domain with full or partial boundary data. Moreover, a rational approximation method in [8] and a method of gradient descent and a

* Corresponding author.
E-mail addresses: xmdeng@oamail.gdufs.edu.cn (X. Deng), liaozj@jnu.edu.cn (Z.-J. Liao), xccai@um.edu.mo (X.-C. Cai).

[1] The first two authors contributed equally to this work.

https://doi.org/10.1016/j.cam.2021.113441
0377-0427/

trust-region-reflective algorithm in [10] are developed to detect the location, size and shape of hidden sources within a body using measurements on external boundaries. In [6] a reduced space approach is developed for piecewise constant sources with different amount of observation data, where the associated Hessian problem is solved by a preconditioned conjugate gradient algorithm. When it comes to determine a general source function, such as the harmonic source [6], or the Gaussian source(s) [5], it usually requires measurements inside the domain and the measurement on the boundary alone is not enough. In [11,12], an algorithmic framework for recovering a general source function is introduced in which the inverse problem is described as a PDE-constrained optimization problem and then solved by a Tikhonov regularization method.

Existing parallel algorithms for solving PDE-constrained optimization problems often focus on developing efficient parallel solvers for the first-order optimality condition, namely the Karush–Kuhn–Tucker (KKT) system consisting of the state equation, the adjoint equation and the source equation. The coupled system of the three equations can be solved either in a three-step sequential iteration [4,13] or simultaneously [14–16]. For example, in [13] for the reconstruction of the medium profile of heterogeneous semi-infinite domains, at each iteration of a conjugate gradient method the state, adjoint and target variables are updated sequentially. In [16] for a distributed Stokes control problem, the KKT system is solved with a preconditioned all-at-once multigrid method. For both methods, the linear systems discretized from the KKT system are large, sparse and ill-conditioned, preconditioning techniques are necessary. In the three-step sequential approaches, three separate parallel preconditioners are applied when solving each of the three equations, however for the all-at-once method, a global preconditioner should be computed for the fully-coupled KKT system. The all-at-once method offers higher degree of parallelism, but usually costs more effort per iteration in terms of forming and applying the preconditioner. Parallel preconditioners include Jacobi or block Jacobi preconditioner, incomplete LU or SOR preconditioner, and the domain decomposition ones such as the additive or multiplicative Schwarz preconditioner and so on [17]. Among these preconditioners, the Schwarz preconditioner is quite suitable for parallel processing, and has been widely applied in PDE-related engineering problems such as the simulation of two-phase flows in porous media [18], the large eddy simulation of high speed trains [19] or the neutron transport criticality calculations [20].

As we know, the scalability of any one-level domain decomposition method deteriorates with increasing number of processors [21], multilevel methods are necessary when the number of processors increases [22–25]. In this paper we propose and study a parallel multilevel domain decomposition method to avoid solving the large KKT system and further reduce the global communication for solving the general source inverse problem. We briefly mention our motivation here. Suppose $f(\mathbf{x})$, $\mathbf{x} \in \Omega$, is the source function to be determined on the domain Ω and the measurements are available at some points in Ω. Let us assume that Ω has two subdomains $\Omega_1 \subset \Omega$ and $\Omega_2 \subset \Omega$, and correspondingly we have $f_1(\mathbf{x})$ defined on Ω_1 and $f_2(\mathbf{x})$ defined on Ω_2. In the classical approach, the inverse problem is formulated as a single optimization problem over Ω. As a result, $f_1(\mathbf{x})$ and $f_2(\mathbf{x})$ would be coupled in a single system. However, in our new approach, $f_1(\mathbf{x})$ and $f_2(\mathbf{x})$ can be recovered independently if Ω_1 and Ω_2 do not overlap. Based on this observation, we propose a domain decomposition method which divide the original optimization problem into smaller subproblems, and the smaller KKT systems corresponding to these subproblems are solved all-at-once independently and simultaneously on the subdomains. Then the solutions of all subdomains are appropriately glued together to form a global solution. A similar idea was used successfully for the denoising of images in [26]. The feasibility of the proposed approach is analyzed here for the continuous formulation of the source inversion problem. Numerical experiments are provided to illustrate the efficiency of the method.

The rest of the paper is arranged as follows: Section 2 first shows the framework of the Tikhonov regularization method, and then the multilevel domain decomposition method is proposed; Section 3 provides some analysis of the existence and well-posedness of the reconstructed solution for the multilevel domain decomposition method; three numerical examples are shown in Section 4 to test the reconstruction effect and the algorithm efficiency. Some conclusions are drawn in Section 5.

2. The multilevel domain decomposition method

We consider the general source inversion problem associated with a variable-coefficient elliptic equation defined on an open, bounded and simply connected domain $\Omega \in \mathbf{R}^2$ with Lipschitz boundary $\partial\Omega$,

$$\begin{cases} -\nabla \cdot (a(\mathbf{x})\nabla u(\mathbf{x})) = f(\mathbf{x}), & \mathbf{x} \in \Omega \\ u(\mathbf{x}) = p(\mathbf{x}), & \mathbf{x} \in \partial\Omega, \end{cases} \tag{1}$$

where $a(\mathbf{x}) \in L^\infty(\Omega)$ and $0 < a_1 \le a(\mathbf{x}) \le a_2$, $f(\mathbf{x})$ denotes the source function to be recovered, and $p(\mathbf{x})$ is a given smooth function for the Dirichlet boundary condition. Many numerical methods are available for solving the forward problem [27–30]. The inverse source identification problem is to recover $f(\mathbf{x})$ in (1) using some given measurement data $u^\epsilon(\mathbf{x})$ of $u(\mathbf{x})$ (ϵ denotes the noise level) at some locations in Ω.

2.1. The Tikhonov regularization method

We briefly recall the Tikhonov regularization method which reformulates the inverse problem as an output least-square optimization problem with a regularization term to ensure the well-posedness of the resulting optimization problem [31]. The objective functional with Tikhonov regularization for the inverse source identification problem reads as: Find f that minimizes

$$J(f) = \frac{1}{2}\int_{\Omega} (u(\mathbf{x}) - u^{\epsilon}(\mathbf{x}))^2 \, d\mathbf{x} + N_{\beta}(f), \tag{2}$$

where $u^{\epsilon}(\mathbf{x}) \in L^2(\Omega)$, $N_{\beta}(f)$ is the Tikhonov regularization appropriately chosen by prior information, such as L^2 or H^1 regularization for continuous source functions or bounded variation regularization for discontinuous sources. For simplicity here we use the following H^1 regularization:

$$N_{\beta}(f) = \frac{\beta}{2}\int_{\Omega} |\nabla f|^2 d\mathbf{x}, \tag{3}$$

with β being the regularization parameter. The admissible function space for the unknown source function f on Ω is defined as M_{Ω}:

$$f \in M_{\Omega} = \{f | f \in H^{-1}(\Omega) \quad \text{and} \quad |f|_{1,\Omega} < \infty\}. \tag{4}$$

Now the inverse source identification problem is equivalent to solving the following optimization problem $\mathcal{P}$ with a PDE constraint (1):

$$\begin{aligned} &\mathcal{P} : \min_{f} J(f), \\ &\quad \text{subject to } (u, f) \text{ satisfying (1)}. \end{aligned} \tag{5}$$

By introducing a Lagrange multiplier or an adjoint function v, we define the following Lagrange functional for (2):

$$\mathcal{J}(u, f, v) = J(f) + (v, Lu - f), \tag{6}$$

where L denotes the elliptic operator of (1), $(\cdot, \cdot)$ is the L^2 inner product. The optimization problem (5) is then transformed into solving an unconstrained optimization problem with the objective functional (6). By computing the Fréchet derivative with respect to the three variables and integrating by parts, a minima of (6) should satisfy the following weak KKT optimality system: $\forall \phi, \psi \in H_0^1(\Omega)$, $\omega \in H^1(\Omega)$, finding $u, f \in H^1(\Omega)$, $v \in H_0^1(\Omega)$ such that

$$\begin{cases} (a(\mathbf{x})\nabla u(\mathbf{x}), \nabla \phi) = (f(\mathbf{x}), \phi), & \mathbf{x} \in \Omega \\ (a(\mathbf{x})\nabla v(\mathbf{x}), \nabla \psi) + (u(\mathbf{x}), \psi) = (u^{\epsilon}(\mathbf{x}), \psi), & \mathbf{x} \in \Omega \\ -(v(\mathbf{x}), \omega) + \beta(\nabla f(\mathbf{x}), \nabla \omega) = 0, & \mathbf{x} \in \Omega. \end{cases} \tag{7}$$

We remark that the computational cost of solving the fully-coupled KKT system (7) can be tremendous. To avoid solving such a large linear system, we propose a parallel domain decomposition algorithm which divides the original optimization problem into several smaller subproblems and then solve these subproblems in parallel.

2.2. A multilevel domain decomposition method

Firstly, we divide the domain Ω into m_1 smaller non-overlapping subdomains $\Omega_1, \Omega_2, \ldots, \Omega_{m_1}$, see Fig. 1 for a sample decomposition of Ω.

Using the decomposition of Ω, the objective functional of (5) can be decomposed as

$$\begin{aligned} J(f) &= \frac{1}{2}\int_{\Omega} (u(\mathbf{x}) - u^{\epsilon}(\mathbf{x}))^2 \, d\mathbf{x} + \frac{\beta}{2}\int_{\Omega} |\nabla f|^2 d\mathbf{x} \\ &= \sum_{i=1}^{m_1} \left\{ \frac{1}{2}\int_{\Omega_i} (u(\mathbf{x}) - u^{\epsilon}(\mathbf{x}))^2 \, d\mathbf{x} + \frac{\beta}{2}\int_{\Omega_i} |\nabla f|^2 d\mathbf{x} \right\}. \end{aligned}$$

The question is if we can decompose the optimization problem (5) into smaller problems defined on Ω_i, $i = 1, 2, \ldots, m_1$. The PDE constraint is satisfied on all subdomains, but an obvious issue is the boundary conditions of the PDE are not always available. Note that after the partition, the boundary of each subdomain Ω_i consists of two types of boundaries: the actual boundary of Ω, denoted by $\partial\Omega$ and the artificial boundary generated by the decomposition, denoted by Γ_i as shown in Fig. 1. At these artificial boundaries Γ_i, appropriate boundary conditions are needed. A natural idea is to use homogeneous boundary conditions, but then we cannot obtain the global solution by combining the solution on each Ω_i. To overcome this problem, we introduce an overlapping decomposition of Ω by extending each Ω_i outward by a layer of size $\delta > 0$, and the overlapping subdomains are denoted by $\Omega_1', \Omega_2', \ldots, \Omega_{m_1}'$. By choosing appropriate overlapping size, after each subproblem is solved on Ω_i', we cut off all the parts of solution in the overlapping region

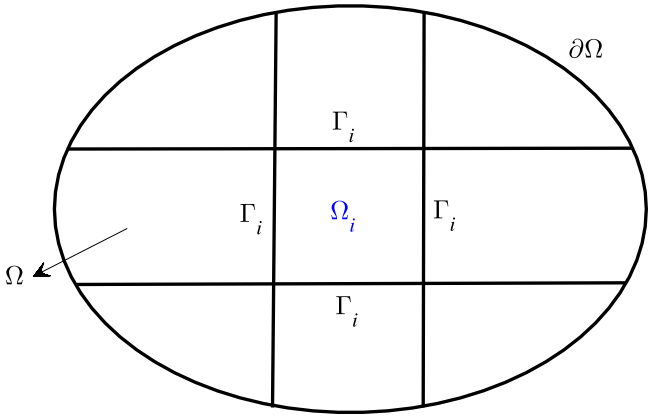

Fig. 1. The domain decomposition of Ω.

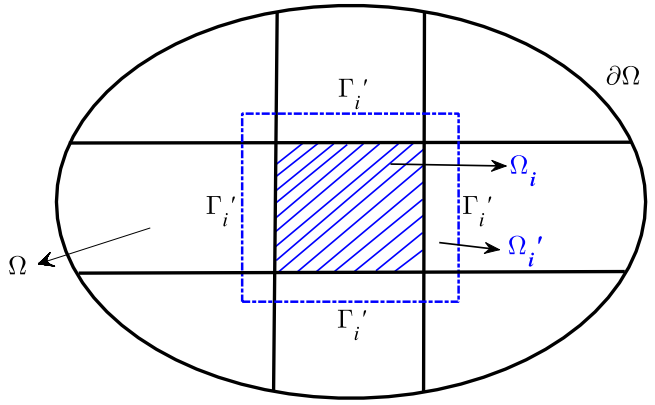

Fig. 2. The first-level overlapping domain decomposition of Ω into Ω_i', $i = 1, \ldots, m_1$.

$\Omega_i' \backslash \Omega_i$ and glue the parts of solution on Ω_i, $i = 1, \ldots, m_1$ together to form an approximate solution of the original problem $\mathcal{P}$. An overlapping version of the domain decomposition is shown in Fig. 2.

With the overlapping domain decomposition, we define an objective functional for each Ω_i'

$$J_i(f_i) = \frac{1}{2}\int_{\Omega_i'} (u_i(\mathbf{x}) - u^{\epsilon}(\mathbf{x}))^2 \, d\mathbf{x} + \frac{\beta}{2}\int_{\Omega_i'} |\nabla f_i|^2 d\mathbf{x}, \tag{8}$$

where u_i and f_i satisfy the following constraint

$$\begin{cases} -\nabla \cdot (a(\mathbf{x})\nabla u_i(\mathbf{x})) = f_i(\mathbf{x}), & \mathbf{x} \in \Omega_i' \\ u_i(\mathbf{x}) = p(\mathbf{x}), & \mathbf{x} \in \partial\Omega_i' \cap \partial\Omega \\ u_i(\mathbf{x}) = 0, & \mathbf{x} \in \Gamma_i'. \end{cases} \tag{9}$$

The subproblems $\mathcal{P}_i'$ on Ω_i', $i = 1, 2, \ldots, m_1$, are defined as:

$$\begin{aligned} &\mathcal{P}_i' : \operatorname*{Min}_{f_i} J_i(f_i), \\ &\quad \text{subject to } (u_i, f_i) \text{ satisfying (9).} \end{aligned} \tag{10}$$

To solve the optimization problem $\mathcal{P}_i'$, we construct and solve the following KKT system: Find $u_i, f_i \in H^1(\Omega_i')$, $v_i \in H_0^1(\Omega_i')$

$$\begin{cases} (a(\mathbf{x})\nabla u_i(\mathbf{x}), \nabla\phi) = (f_i(\mathbf{x}), \phi), & \mathbf{x} \in \Omega_i' \\ (a(\mathbf{x})\nabla v_i(\mathbf{x}), \nabla\psi) + (u_i(\mathbf{x}), \psi) = (u^{\epsilon}(\mathbf{x}), \psi), & \mathbf{x} \in \Omega_i' \\ -(v_i(\mathbf{x}), \omega) + \beta(\nabla f_i(\mathbf{x}), \nabla\omega) = 0, & \mathbf{x} \in \Omega_i' \end{cases} \tag{11}$$

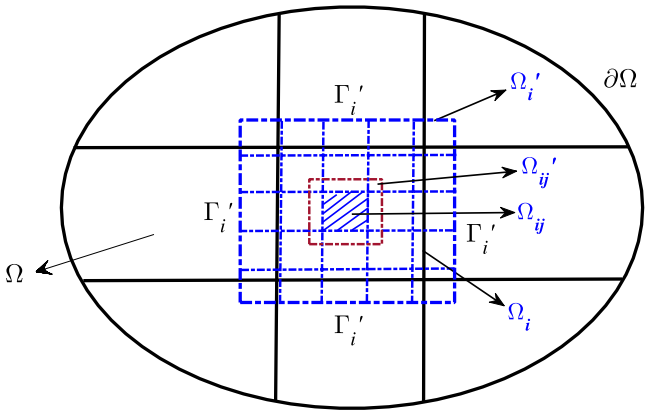

Fig. 3. The second-level overlapping domain decomposition inside each subdomain Ω_i' into Ω_{ij}', $i = 1, \ldots, m_1$, $j = 1, \ldots, m_2$.

$\forall \phi, \psi \in H_0^1(\Omega_i')$, $\omega \in H^1(\Omega_i')$. The boundary conditions for the state variable (i.e. u_i) are given by (9). By the arbitrariness of ψ, the boundary condition for v_i has to be:

$$v_i(\mathbf{x}) = 0, \quad \mathbf{x} \in \partial\Omega_i'.$$

Similarly using the arbitrariness of ω, we obtain the homogeneous Neumann boundary condition for f_i as:

$$\frac{\partial f_i}{\partial \mathbf{n}} = 0 \quad \text{for } \mathbf{x} \in \partial\Omega_i'.$$

2.3. A parallel domain decomposition based finite element solver

In this section we introduce a parallel domain decomposition based finite element method for solving (11). Each subdomain Ω_i', $i = 1, \ldots, m_1$ is partitioned into quasi-uniform conforming triangular elements denoted by $\mathcal{T}_i^h$, with h being the element size. On $\mathcal{T}_i^h$ we define a piecewise linear continuous finite element space V_i^h, and its subspace $\mathring{V}_i^h$ with zero trace on $\partial\Omega_i'$. Let π^h be the finite element interpolation associated with V_i^h, then (11) is transformed into the following discrete problem: Find $u_i^h, f_i^h \in V_i^h$, $v_i^h \in \mathring{V}_i^h$, such that $u_i^h = \pi^h p(\mathbf{x})$ on $\partial\Omega_i' \cap \partial\Omega$, $u_i^h = \pi^h 0$ on Γ_i', and

$$\begin{cases} (a(\mathbf{x})\nabla u_i^h(\mathbf{x}), \nabla \phi^h) = (f_i^h(\mathbf{x}), \phi^h), & \mathbf{x} \in \Omega_i' \\ (a(\mathbf{x})\nabla v_i^h(\mathbf{x}), \nabla \psi^h) + (u_i^h(\mathbf{x}), \psi^h) = (u^{\epsilon,h}(\mathbf{x}), \psi^h), & \mathbf{x} \in \Omega_i' \\ -(v_i^h(\mathbf{x}), \omega^h) + \beta(\nabla f_i^h(\mathbf{x}), \nabla \omega^h) = 0, & \mathbf{x} \in \Omega_i', \end{cases} \tag{12}$$

for all $\phi^h, \psi^h \in \mathring{V}_i^h$ and $\omega^h \in V_i^h$. The discrete form of (12) is denoted as

$$K_i U_i = B_i, \tag{13}$$

where K_i is the fully coupled finite element stiffness matrix, and U_i is the collections of unknowns with the three variables on the same node arranged together as follows

$$U_i = (u_i^1, v_i^1, f_i^1, \ldots, u_i^j, v_i^j, f_i^j, \ldots, u_i^{N_i}, v_i^{N_i}, f_i^{N_i}),$$

where N_i is the number of nodes, and B_i is the corresponding right-hand side vector.

We apply a Krylov subspace method with a right Schwarz preconditioner to solve the system (13). More precisely speaking, to find U_i, we solve

$$K_i M_i^{-1} U_i' = B_i, \qquad U_i = M_i^{-1} U_i'.$$

To construct the Schwarz preconditioner M_i^{-1}, a second level of overlapping domain decomposition inside each subdomain Ω_i', $i = 1, 2, \ldots, m_1$ is performed. See Fig. 3 for an example.

Suppose Ω_i' is decomposed into m_2 overlapping subdomains, the restricted additive Schwarz preconditioner (RAS) [32] of K_i, denoted by M_i^{-1}, can be constructed as follows:

$$M_i^{-1} = \sum_{j=1}^{m_2} (R_{ij}^\tau)^T \tilde{K}_{ij}^{-1} R_{ij}^0, \tag{14}$$

where $(R_{ij}^{\tau})^T$ denotes the restriction matrix from Ω_i' to the subdomain Ω_{ij}' (τ being the overlapping size) and the transpose of the restriction matrix without overlap (denoted by R_{ij}^0) is used as the interpolation matrix, $\tilde{K}_{ij}^{-1}$ is the approximate inverse of the subproblem corresponding to the subdomain Ω_{ij}'.

In the parallel implementation of the algorithm, each problem associated with a Ω_{ij}', $i = 1, \ldots, m_1$, $j = 1, \ldots, m_2$ is allocated to a processor, the total number of processor cores that we need is $np = m_1 m_2$. The advantage of the proposed algorithm lies in two aspects. Firstly the multilevel domain decomposition method has no communication cost between adjacent subdomains Ω_i' and Ω_k' ($i \neq k$), parallel communication only happens inside each subdomain Ω_i'. The subproblems on Ω_i', $i = 1, \ldots, m_1$ are independent of each other and thus can be solved in parallel. It is noted that if the scale of the subproblem $\mathcal{P}_i'$ is small enough to be computed by one processor, then the second level of domain decomposition is not necessary. Secondly if the available number of processors $np < m_1 m_2$, the proposed algorithm is still possible to implement. We divide the np processor cores into at most m ($m < m_1$) groups, with each group assigned with m_2 processors. Then m subproblems are treated as a batch and solved at a time until all the subproblems are solved. The strategy enables us to flexibly handle large-scale problems.

3. Error analysis

In this section, we show the existence of a minimizer to the optimization problem (10) and the error estimate between the solutions of (10) and the solution of the global optimization problem (5). From the standard elliptic theory we know that there exists a unique weak solution to (1), and the solution satisfies:

Lemma 3.1. *The weak solution of the elliptic equation (1) satisfies the following estimate:*

$$\|u\|_{1,\Omega} \leq \frac{C}{a_1}\|f\|_{-1,\Omega} + \left(\frac{Ca_2}{a_1} + 1\right)\|p\|_{\frac{1}{2},\partial\Omega} \tag{15}$$

where C is a positive constant and a_1 and a_2 are upper and lower bounds of the diffusion coefficient $a(\mathbf{x})$.

The detailed proof of this lemma is given in the appendix. Next we show the existence of a minimizer to the optimization problem (10).

Theorem 3.2. *There exists a minimizer to the optimization problem (10) on each subdomain Ω_i'.*

Proof of Theorem 3.2. Using a similar proof of Lemma 3.1 we see that the solution u_i of (9) is bounded in $H^1(\Omega_i')$. Let f_i be the right-hand side of (9), and $f_i^n \in H^1(\Omega_i')$ be a sequence that converges to f_i. Assuming that u_i^n is the corresponding solution of (9) for each f_i^n, we can extract a weakly convergent sequence, still denoted by u_i^n, such that $u_i^n \rightharpoonup u_i^*$ as $n \to \infty$. Below we show $u_i^* = u_i$. Since

$$\begin{aligned}(a(\mathbf{x})\nabla u_i^n, \nabla\phi) &= (f_i^n, \phi), \quad \forall\phi \in H_0^1(\Omega_i')\\ (a(\mathbf{x})\nabla u_i^*, \nabla\phi) - (f_i, \phi) &= -(a(\mathbf{x})\nabla(u_i^n - u_i^*), \nabla\phi) + (f_i^n - f_i, \phi),\end{aligned}$$

by the weak convergence of u_i^n, the assumed convergence on f_i^n and the Cauchy–Schwarz inequality, the right-hand side goes to zero as $n \to \infty$. So we obtain the following equation,

$$(a(\mathbf{x})\nabla u_i^*, \nabla\phi) = (f_i, \phi), \quad \forall\phi \in H_0^1(\Omega_i'),$$

which implies $u_i^* = u_i$.

In the optimization functional of (10), the first data-fitting term of $J_i(f_i)$ satisfies

$$\begin{aligned}\int_{\Omega_i'} (u_i^n - u^\epsilon)^2 d\mathbf{x} &= \int_{\Omega_i'} \left(u_i^n - u_i + u_i - u^\epsilon\right)^2 d\mathbf{x},\\ &= \int_{\Omega_i'} \left(u_i^n - u_i\right)^2 d\mathbf{x} + 2\int_{\Omega_i'} \left(u_i^n - u_i\right)(u_i - u^\epsilon)\, d\mathbf{x}\\ &\quad + \int_{\Omega_i'} (u_i - u^\epsilon)^2\, d\mathbf{x}\\ &\equiv: R_n^1 + R_n^2 + R^3.\end{aligned}$$

By Rellich's theorem (cf. [33], pages 288–291) that $H^1(\Omega_i') \Subset L^2(\Omega_i')$, there exists a subsequence of u_i^n, still denoted by u_i^n, converges strongly to u_i in $L^2(\Omega_i')$, so R_n^1 vanishes as $n \to \infty$. The second term R_n^2 goes to zero by the Cauchy–Schwarz inequality, thus we have

$$\lim_{n\to\infty} \int_{\Omega_i'} (u_i^n - u^\epsilon)^2 dx = \int_{\Omega_i'} (u_i - u^\epsilon)^2 dx. \tag{16}$$

By the boundedness of u_i, the optimization functional $J_i(f_i)$ in (10) is finite over the admissible set defined on Ω_i' by (4), denoted by $M_{\Omega_i'}$. There exists a minimizing sequence f_i^n such that

$$\lim_{n\to\infty} J_i(f_i^n) = \operatorname*{Min}_{f_i\in M_{\Omega_i'}} J_i(f_i).$$

Since $N_\beta(f_i^n)$ is bounded by the definition of $J_i(f_i)$, there exists a subsequence, still denoted by f_i^n, with $f_i^n \to f_i^*$ in $L^2(\Omega_i')$ and $f_i^* \in M_{\Omega_i'}$. Furthermore by (16) and the lower semi-continuity of the H^1 norm, we obtain

$$\begin{aligned} J_i(f_i^*) &\le \lim_{n\to\infty} \frac{1}{2}\int_{\Omega_i'} (u_i^n - u^\epsilon)^2 dx + \frac{\beta}{2} \lim_{n\to\infty} \inf \int_{\Omega_i'} |\nabla f_i^n|^2 dx \\ &\le \lim_{n\to\infty} \inf J_i(f_i^n) = \operatorname*{Min}_{f_i\in M_{\Omega_i'}} J_i(f_i), \end{aligned}$$

which implies $J_i(f_i^*) = \operatorname*{Min}_{f_i\in M_{\Omega_i'}} J_i(f_i)$ and f_i^* is a minimizer of $J_i(f_i)$.

Now we are ready to give the main theorem that provides an error estimate of the reconstructed source function f defined in each non-overlapping subdomain Ω_i, $i = 1, \ldots, m_1$. It is easy to see that the proposed algorithm has an error inherited from the forward model, which is described as follows: denoting $\tilde{u}$ and u_i as the solution of (1) and (9) respectively, we define the error function $\delta u_i = \tilde{u}_i - u_i$, with $\tilde{u}_i \triangleq \tilde{u}|_{\Omega_i'}$ being $\tilde{u}$ restricted in Ω_i', then δu_i satisfies the following equation:

$$\begin{cases} -\nabla\cdot(a\nabla\delta u_i) = 0, & \mathbf{x}\in\Omega_i' \\ \delta u_i(\mathbf{x}) = 0, & \mathbf{x}\in\partial\Omega_i'\cap\partial\Omega \\ \delta u_i(\mathbf{x}) = \delta p_i(\mathbf{x}), & \mathbf{x}\in\Gamma_i', \end{cases} \tag{17}$$

where δp_i denotes the difference between the boundary conditions (or more precisely the trace) of $\tilde{u}_i$ and u_i on the inner boundary Γ_i'.

Theorem 3.3. *The combined solutions of (10), the regularized solution of the original optimization problem (5) and the exact source function are denoted by f, $\tilde{f}^\beta$, and f^* respectively, then*

$$\|f - \tilde{f}^\beta\|_{1,\Omega} \le \frac{C_1 m_1}{\beta a_1} \operatorname*{Max}_{1\le i\le m_1} \|\delta p_i\|_{0,\Gamma_i'}, \tag{18}$$

where C_1 is a constant. Since $\|u - u^\epsilon\|_{0,\Omega} < \epsilon$, if the following conditions are satisfied

$$\operatorname*{Max}_{1\le i\le m_1} \|\delta p_i\|_{0,\Gamma_i'} = O(\epsilon), \qquad \lim_{\epsilon\to 0}\beta = 0, \qquad \lim_{\epsilon\to 0}\frac{\epsilon}{\beta} = 0,$$

then

$$\lim_{\epsilon\to 0} \|f - f^*\|_{1,\Omega} = 0.$$

Proof of Theorem 3.3. We denote the elliptic equation (9) as $Lu_i = f_i$. By introducing a Lagrange multiplier v_i, the optimization functional $J_i(f_i)$ is revised as

$$\begin{aligned} \mathcal{J}_i(u_i, v_i, f_i) &= J_i(f_i) + \langle v_i, Lu_i - f_i\rangle \\ &= \frac{1}{2}(u_i - u^\epsilon, u_i - u^\epsilon) + \frac{\beta}{2}(\nabla f_i, \nabla f_i) + \langle v_i, Lu_i - f_i\rangle. \end{aligned} \tag{19}$$

Since

$$\langle v_i, Lu_i - f_i\rangle = (v_i, Lu_i) - (v_i, f_i) = (L^* v_i, u_i) - (v_i, f_i),$$

taking the Fréchet derivative of (19) and integrating by parts, it is easy to see that $L^* v_i = -\nabla\cdot(a\nabla v_i) = Lv_i$ in $H_0^1(\Omega_i')$, and we obtain the strong formulation of the KKT system of (19) as

$$\begin{cases} Lu_i - f_i = 0 \\ L^* v_i + u_i - u^\epsilon = 0 \\ v_i + \beta\Delta f_i = 0, \end{cases} \tag{20}$$

with appropriate boundary conditions derived in Section 2. From the second equation of (20) we obtain

$$v_i = -(L^*)^{-1}(u_i - u^\epsilon). \tag{21}$$

Denoting the regularized solution of the original optimization problem (5) restricted in Ω_i' as $\tilde{f}_i^\beta$ and $\tilde{u}_i$, we substitute (21) into the third equation of (20), f_i satisfies

$$\begin{aligned}
&-(L^*)^{-1}(u_i-u^\epsilon)+\beta\Delta f_i=0\\
\Rightarrow&-(L^*)^{-1}(u_i-\tilde{u}_i+\tilde{u}_i-u^\epsilon)+\beta\Delta(f_i-\tilde{f}_i^\beta+\tilde{f}_i^\beta)=0\\
\Rightarrow&-(L^*)^{-1}(\tilde{u}_i-u^\epsilon)+\beta\Delta\tilde{f}_i^\beta-(L^*)^{-1}(u_i-\tilde{u}_i)+\beta\Delta(f_i-\tilde{f}_i^\beta)=0.
\end{aligned}$$

From the definition of $\tilde{f}_i^\beta$ we have

$$-(L^*)^{-1}(\tilde{u}_i-u^\epsilon)+\beta\Delta\tilde{f}_i^\beta=0, \tag{22}$$

which implies

$$\begin{aligned}
&-(L^*)^{-1}(u_i-\tilde{u}_i)+\beta\Delta(f_i-\tilde{f}_i^\beta)=0\\
\Rightarrow&f_i-\tilde{f}_i^\beta=\frac{1}{\beta}\Delta^{-1}(L^*)^{-1}(u_i-\tilde{u}_i).
\end{aligned}$$

Note that $\tilde{u}_i-u_i=\delta u_i$ in (17), then

$$f_i-\tilde{f}_i^\beta=-\frac{1}{\beta}\Delta^{-1}(L^*)^{-1}\delta u_i. \tag{23}$$

By the Poincaré's inequality (cf. [33], page 291) and Lemma 3.1, we obtain the following estimate

$$\begin{aligned}
\|f_i-\tilde{f}_i^\beta\|_{1,\Omega_i'}&=\frac{1}{\beta}\|\Delta^{-1}(L^*)^{-1}\delta u_i\|_{1,\Omega_i'}\le\frac{1}{\beta}\|\Delta^{-1}\|_{1,\Omega_i'}\|(L^*)^{-1}\delta u_i\|_{1,\Omega_i'}\\
&\le\frac{C}{\beta a_1}\|\delta u_i\|_{-1,\Omega_i'},
\end{aligned}$$

where C is a constant. By Eq. (17) which is satisfied by δu_i, and the estimate for the trace operator (cf. [34] Lemma 2.4, page 326), we have

$$\|f_i-\tilde{f}_i^\beta\|_{1,\Omega_i'}\le\frac{C}{\beta a_1}\|\delta p_i\|_{-\frac{1}{2},\Gamma_i'}. \tag{24}$$

Since $L^2(\Gamma_i')\Subset H^{-\frac{1}{2}}(\Gamma_i')$ (cf. [35], page 98), then

$$\|f_i-\tilde{f}_i^\beta\|_{1,\Omega_i'}\le\frac{C}{\beta a_1}\|\delta p_i\|_{0,\Gamma_i'}. \tag{25}$$

Summing up the error in m_1 non-overlapping subdomains, we obtain

$$\begin{aligned}
\|f-\tilde{f}^\beta\|_{1,\Omega}&\le\sum_{i=1}^{m_1}\|f-\tilde{f}^\beta\|_{1,\Omega_i},\\
&\le\frac{Cm_1}{\beta a_1}\operatorname*{Max}_{1\le i\le m_1}\|\delta p_i\|_{0,\Gamma_i'}.
\end{aligned}$$

Next we estimate $\|\tilde{f}^\beta-f^*\|_{1,\Omega}$. We substitute $\tilde{u}_i=L^{-1}\tilde{f}_i^\beta$ to (22) and obtain

$$\begin{aligned}
&-(L^*)^{-1}(L^{-1}\tilde{f}_i^\beta-u^\epsilon)+\beta\Delta\tilde{f}_i^\beta=0,\\
\Rightarrow&\tilde{f}_i^\beta=((LL^*)^{-1}-\beta\Delta)^{-1}(L^*)^{-1}u^\epsilon.
\end{aligned}$$

Since $\forall\phi\in H_0^1(\Omega)$, $((LL^*)^{-1}\phi,\phi)=(L^{-1}\phi,L^{-1}\phi)\ge 0$, by Poincaré's inequality

$$(((LL^*)^{-1}-\beta\Delta)\phi,\phi)\ge\beta(-\Delta\phi,\phi)\ge C\beta\|\phi\|_{1,\Omega_i'}^2, \tag{26}$$

by Lax–Milgram theorem (cf. [33], pages 317–319), there exists $((LL^*)^{-1}-\beta\Delta)^{-1}$ and

$$\|((LL^*)^{-1}-\beta\Delta)^{-1}\|\le\frac{C}{\beta}. \tag{27}$$

If we denote the exact data without measurement noise as u^0, and the regularized solution with exact data as $(\tilde{f}_i^*)^\beta$, then

$$\begin{aligned}
&\tilde{f}_i^\beta-(\tilde{f}_i^*)^\beta=((LL^*)^{-1}-\beta\Delta)^{-1}(L^*)^{-1}(u^\epsilon-u^0)\\
\Rightarrow&\|\tilde{f}_i^\beta-(\tilde{f}_i^*)^\beta\|\le\|((LL^*)^{-1}-\beta\Delta)^{-1}\|\|(L^*)^{-1}(u^\epsilon-u^0)\|\\
\Rightarrow&\|\tilde{f}_i^\beta-(\tilde{f}_i^*)^\beta\|_{1,\Omega_i'}\le\frac{C}{\beta a_1}\|(u^\epsilon-u^0)\|_{-1,\Omega_i'}.
\end{aligned}$$

Since $H^1(\Omega_i') \Subset L^2(\Omega_i')$, by Schauder's theorem (cf. [36], Theorem 4.19, page 105) $L^2(\Omega_i') \Subset H^{-1}(\Omega_i')$, thus $\|(u^\epsilon - u^0)\|_{-1,\Omega_i'} \leq C\|(u^\epsilon - u^0)\|_{0,\Omega_i'} < C\epsilon$ and

$$\|\tilde{f}_i^\beta - (\tilde{f}_i^*)^\beta\|_{1,\Omega_i'} < \frac{C\epsilon}{a_1\beta}, \tag{28}$$

As a result, by the Cauchy–Schwarz inequality,

$$\begin{aligned}\|f - f^*\|_{1,\Omega} &\leq \sum_{i=1}^{m_1} \left(\|f_i - \tilde{f}_i^\beta\|_{1,\Omega_i} + \|\tilde{f}_i^\beta - (\tilde{f}_i^*)^\beta\|_{1,\Omega_i} + \|(\tilde{f}_i^*)^\beta - f_i^*\|_{1,\Omega_i} \right) \\ &\leq \frac{C_1 m_1}{\beta a_1} \max_{1\leq i\leq m_1} \|\delta p_i\|_{0,\Gamma_i'} + \frac{C_2 m_1 \epsilon}{a_1\beta} + \sum_{i=1}^{m_1} \|(\tilde{f}_i^*)^\beta - f_i^*\|_{1,\Omega_i},\end{aligned}$$

with C_1 and C_2 being the corresponding constants after discarding the overlapping part $\Omega_i'\backslash\Omega_i$. By the regularization theory [31], the last term satisfies $\lim_{\beta\to 0} \|(\tilde{f}_i^*)^\beta - f_i^*\|_{1,\Omega_i} = 0$ for $i = 1, \ldots, m_1$, so if

$$\max_{1\leq i\leq m_1} \|\delta p_i\|_{0,\Gamma_i'} = O(\epsilon), \qquad \lim_{\epsilon\to 0} \beta = 0, \qquad \lim_{\epsilon\to 0} \frac{\epsilon}{\beta} = 0,$$

then

$$\|f - f^*\|_{1,\Omega} \lesssim \frac{m_1}{a_1}\frac{\epsilon}{\beta} \to 0 \qquad (\epsilon \to 0). \tag{29}$$

Remarks.

(1) We remark that Theorem 3.3 shows that the collection of the sub-optimization problems is well-posed and the solutions depend continuously on the measurement data as long as the error from the inexact artificial boundary conditions can be controlled at the same level as the level of noise. This estimate will be further illustrated by several numerical experiments.

(2) C_1 and C_2 are two constants related to the overlapping size δ. Since we only keep the part of the solution in the non-overlapping subdomain Ω_i and count the corresponding error in Ω_i, increasing the overlapping size implies larger distance to the artificial boundaries Γ_i' and less area ratio of Ω_i versus Ω_i'. Therefore both C_1 and C_2 would decrease with the increase of the overlapping size.

(3) Theorem 3.3 implies that there are two ways to reduce the reconstruction error. If homogeneous boundary conditions are applied on Γ_i', then the overlapping size should be relatively large. On the other hand we can impose a more accurate boundary condition on Γ_i', such as using the measurement data with a small noise level, in this case the condition $\max_{1\leq i\leq m_1} \|\delta p_i\|_{0,\Gamma_i'} = O(\epsilon)$ of Theorem 3.3 is satisfied, and the numerical solution can be improved. We will test the schemes with both types of boundary conditions in our numerical experiments.

4. Numerical experiments

In this section we present several numerical experiments to show the accuracy, the robustness and the parallel efficiency of the proposed algorithm. Firstly, we focus on the error of the reconstruction with respect to different levels of noise, the amount of measurement data, the overlapping size, and different boundary conditions on the artificial boundaries. Secondly, we study the parallel performance with different number of subdomains m_1 and m_2, and we also compare the proposed algorithm with the classical approach without any domain decomposition, i.e. $m_1 = 1$.

The computational domain is $\Omega = [-L, L] \times [-H, H]$ with $L = H = 10.0$, the diffusion coefficient is $a(x, y) = 3.0 + \frac{x-y}{L}$, and the Dirichlet boundary condition is $p(x, y) = 1.0$. We define the first-level overlapping size by a parameter θ, which equals to the ratio of the actual overlap versus the subdomain width. In the numerical experiments $\theta = 0.5$ is used if not otherwise specified. At the second level of domain decomposition, the overlapping sizes in both the x- and y- directions are equal to $2h$, with h being the mesh size. The linear systems in (13) are solved by the restarted GMRES method. The restart number is set to 50 and the relative tolerance is 10^{-6}. Homogeneous boundary conditions are imposed on Γ_i', $i = 1, 2, \ldots, m_1$ if not otherwise mentioned. The average number of GMRES iterations is denoted as *its*, and the average time of computation is denoted as Time(s) in seconds. To measure the error of the recovered source function, we use the following relative error function

$$E = \sqrt{\frac{\sum_{i=1}^N (f(\mathbf{x}_i) - f^*(\mathbf{x}_i))^2}{\sum_{i=1}^N (f^*(\mathbf{x}_i))^2}},$$

where N is the total number of mesh points in all non-overlapping subdomains.

We test the following three examples of source functions.

Table 1
The numerical results with different level of data noise ϵ.

Ex1				
ϵ	β	*its*	Time (s)	*E*
1%	10^{-4}	26	0.3830	0.0342
3%	10^{-4}	26	0.3829	0.0806
5%	10^{-3}	54	0.7480	0.1076
10%	10^{-3}	54	0.7397	0.2001
Ex2				
ϵ	β	*its*	Time (s)	*E*
1%	10^{-5}	14	0.2373	0.0151
3%	10^{-4}	27	0.3895	0.0255
5%	10^{-4}	27	0.3828	0.0398
10%	10^{-3}	55	0.7450	0.0772
Ex3				
ϵ	β	*its*	Time (s)	*E*
1%	10^{-5}	14	0.2423	0.0606
3%	10^{-5}	14	0.2380	0.0771
5%	10^{-4}	26	0.3823	0.1004
10%	10^{-3}	55	0.7623	0.1525

Example 1. The source function is a composition of four Gaussian sources:

$$f(x,y)=\sum_{i=0}^{3} b_i e^{-((x-x_i^*)^2+(y-y_i^*)^2)/a_i^2},$$

with $\{a_i\}=\{4,2,3,4\}$, $\{b_i\}=\{4,3,2,5\}$, and $\{(x_i^*,y_i^*)\}=\{(-2.2774,-3.4954),(6.1803,6.1803),(-6.1803,-6.1803),(-8.8444,8.8444)\}$.

Example 2. A polynomial source:

$$f(x,y)=(x+y-0.4L)(y-0.4L)+(x+y+0.4H)(x+0.4H)+20.$$

Example 3. A piecewise constant source:

$$f(x,y)=\begin{cases}6.0, & \text{if } (x-0.5L)^2+(y+0.5H)^2\le 0.4L\\ 6.0, & \text{if } (x+0.5L)^2+(y-0.5H)^2\le 0.4L\\ 3.0, & \text{otherwise.}\end{cases}$$

4.1. Experiments with varying noise level

We partition Ω into four subdomains in a checker board fashion. The measurement data is generated by numerically solving the forward problem on a very fine mesh 385×385. We then restrict the solution to a $m\times m$ coarse mesh on each Ω_i'. The Gaussian noise is added to the solution at the measurement points $\mathbf{x}_i$ as follows:

$$u^{\epsilon}(\mathbf{x}_i)=u(\mathbf{x}_i)+\epsilon\,\sigma\,u(\mathbf{x}_i),\quad i=1,\ldots,m^2.$$

Here σ is a random function satisfying the standard Gaussian distribution and ϵ is the noise level. To discretize $\mathcal{P}_i'$, we use a $m'\times m'=97\times 97$ mesh and the measurement data ratio of m versus m' is denoted as r. In this experiment we set the measurement data ratio to be $r=\frac{1}{4}$.

Note that the mesh for the measurement data and the mesh for the inverse algorithm are not nested. We consider several noise levels $\epsilon=1\%,3\%,5\%,10\%$ and the regularization parameters β are chosen heuristically from six candidates 10^{-1}, 10^{-2}, 10^{-3}, 10^{-4}, 10^{-5}, and 10^{-6}. The results are summarized in Table 1. The reconstructed source function with different noise levels is shown in Figs. 4–6. As expected, when the level of noise is small, the error is small. The error for Example 2 is smaller than that for Examples 1 and 3 at all levels, thus the algorithm works better for polynomial source function. Moreover the number of GMRES iterations and the computing time increase significantly especially for $\epsilon=5\%$ or 10%.

4.2. Experiments with varying amount of measurement data

In this set of experiments we fix the level of noise to 1% and decrease the amount of measurement data. The mesh and overlap are the same as in the previous experiment. The ratio of measurements is reduced to $r=\frac{1}{6},\frac{1}{8}$ and $\frac{1}{12}$, and the

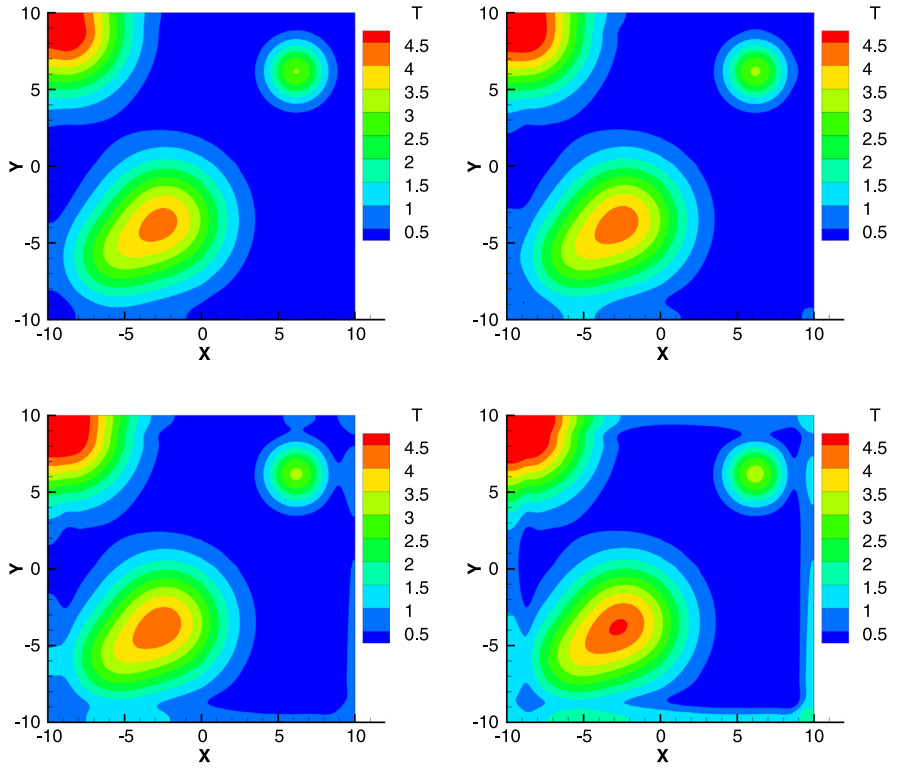

Fig. 4. Example 1: The comparison of reconstructed source function at the noise level $\epsilon = 1\%$ (top left), 3% (top right), 5% (bottom left), and 10% (bottom right).

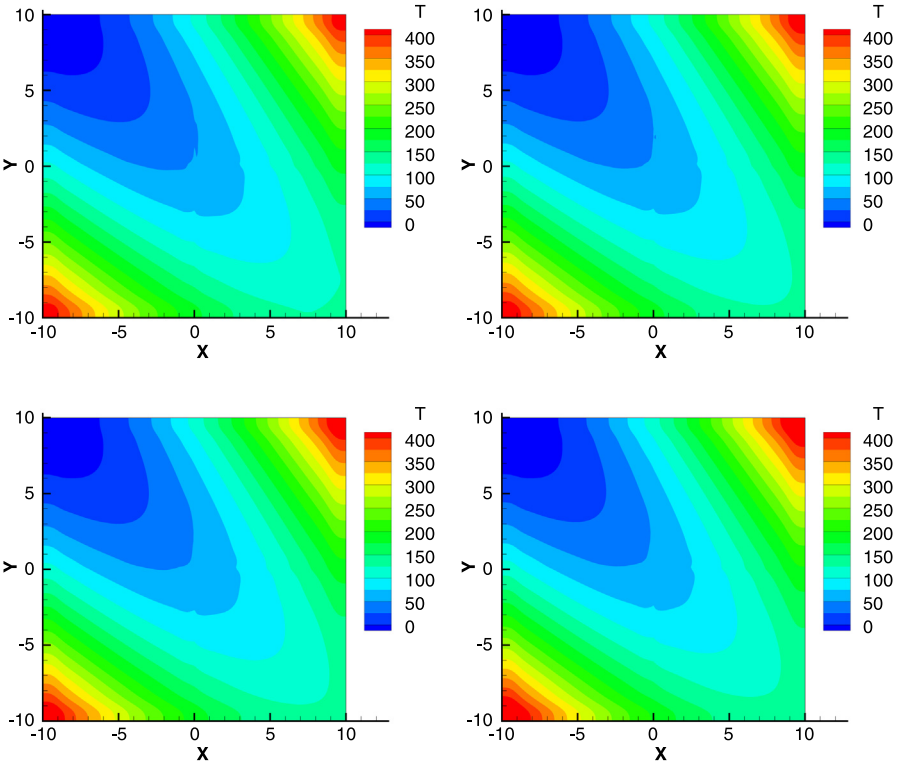

Fig. 5. Example 2: The comparison of reconstructed source function at the noise level $\epsilon = 1\%$ (top left), 3% (top right), 5% (bottom left), and 10% (bottom right).

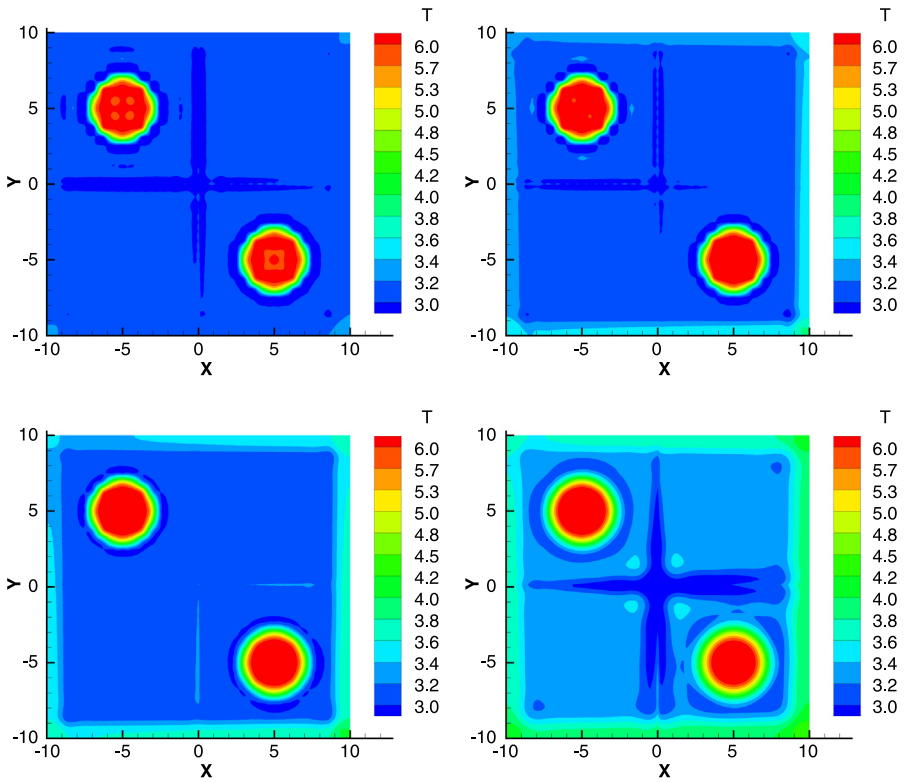

Fig. 6. Example 3: The comparison of reconstructed source function at the noise level $\epsilon = 1\%$ (top left), 3% (top right), 5% (bottom left), and 10% (bottom right).

Table 2
The numerical results with decreasing amount of measurement data.

Ex1				
r	β	*its*	Time (s)	E
$\frac{1}{6}$	10^{-3}	69	0.8994	0.0489
$\frac{1}{8}$	10^{-3}	77	1.0037	0.0794
$\frac{1}{12}$	10^{-3}	91	1.1653	0.2357
Ex2				
r	β	*its*	Time (s)	E
$\frac{1}{6}$	10^{-4}	35	0.4837	0.0307
$\frac{1}{8}$	10^{-3}	78	1.0074	0.0677
$\frac{1}{12}$	10^{-3}	90	1.1789	0.1822
Ex3				
r	β	*its*	Time (s)	E
$\frac{1}{6}$	10^{-4}	35	0.5075	0.0768
$\frac{1}{8}$	10^{-3}	76	0.9979	0.1193
$\frac{1}{12}$	10^{-3}	90	1.1649	0.2974

corresponding meshes for the measurement data are 16×16, 12×12 and 8×8 on each subdomain. The regularization parameter is chosen heuristically. The results are shown in Table 2 and Figs. 7–9. As is shown, the solution error, the number of GMRES iterations and the computing time increase with decreasing amount of measurement data. Moreover the resolution of the reconstructed source becomes worse with less measurement data, large oscillations are observed at the internal subdomain edges for the case of $r = \frac{1}{12}$.

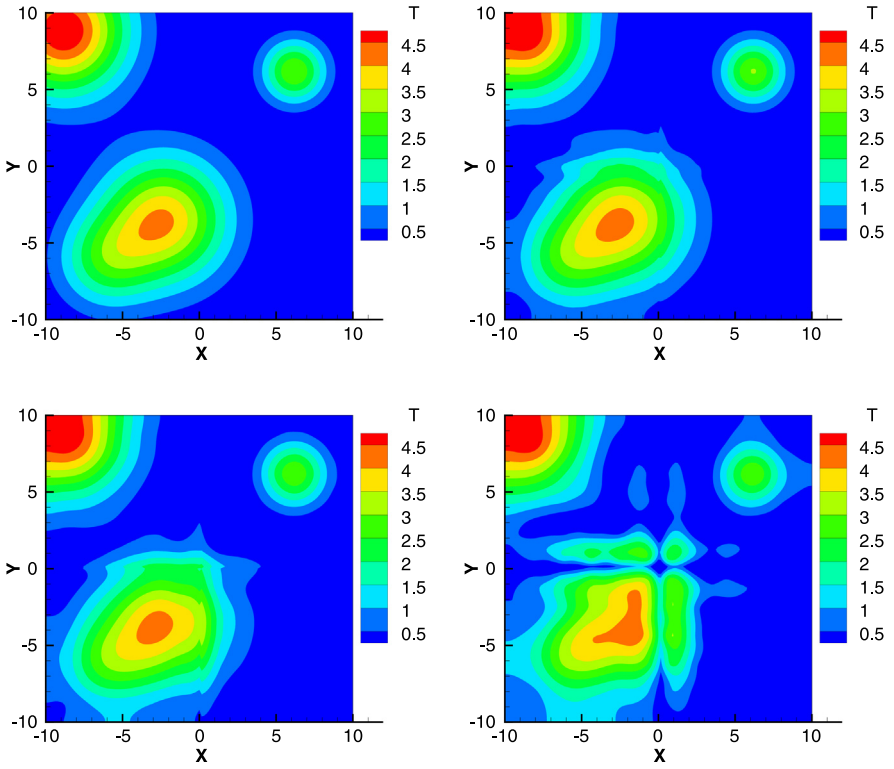

Fig. 7. Example 1: The comparison of the exact source function (top left) with the reconstructed source function with the measurement data ratio $r = \frac{1}{6}$ (top right), $\frac{1}{8}$ (bottom left), $\frac{1}{12}$ (bottom right).

4.3. Experiments with varying overlapping size

In this experiment we investigate how the reconstruction error changes with different overlapping sizes determined by the ratio θ under the same settings as in Section 4.1. It is noted that although the overlapping size changes, we keep the mesh the same as in Section 4.1. We plot the error E of the three examples with θ changing from 0.1 to 0.98 in Fig. 10. It is observed that at the beginning the error decreases quickly with the increasing overlapping size. However when θ reaches about $\frac{1}{3}$, the solution errors of the three examples decrease very slowly and stay almost still despite increasing θ. This tells us $\theta \approx \frac{1}{3}$ is good enough to obtain a reasonable solution. Larger overlap is not necessary.

4.4. Comparison of two boundary conditions

As analyzed earlier, if we use the measurement data as the boundary condition on Γ_i', we expect better reconstruction result and require smaller overlap than that using homogeneous boundary conditions. In this test we substitute the homogeneous conditions with noisy measurement data on every mesh point on Γ_i'. We set the number of subdomains $m_1 = 16$ for Examples 1–3. The length and width of each non-overlapping subdomain is $\frac{2L}{4} = 5.0$. The mesh used for each subproblem is 61×61 and the measurement data ratio is $r = \frac{1}{4}$. Columns 3, 5, 7 of Table 3 show the reconstruction errors using homogeneous boundary conditions (denoted by E_0) with increasing overlap ratio θ and noise level ϵ for Examples 1–3 respectively. Moreover we list the errors of using noisy measurement data on Γ_i' (denoted by E_ϵ) in Columns 4, 6, 8 for comparison. It is observed from Table 3 that when $\theta < 0.3$, the algorithm fails to obtain reasonable solutions with homogeneous boundary conditions. The solutions obtained by using noisy measurement values on the artificial boundaries are much better, even with 10% data noise and a small overlap. If we increase the overlap ratio to $\theta = 0.4$ and $\theta = 0.5$, and apply large enough overlap, the error gap between the two boundary conditions is much narrowed, and the algorithm of using measurement data slightly outperforms that with homogeneous boundary conditions.

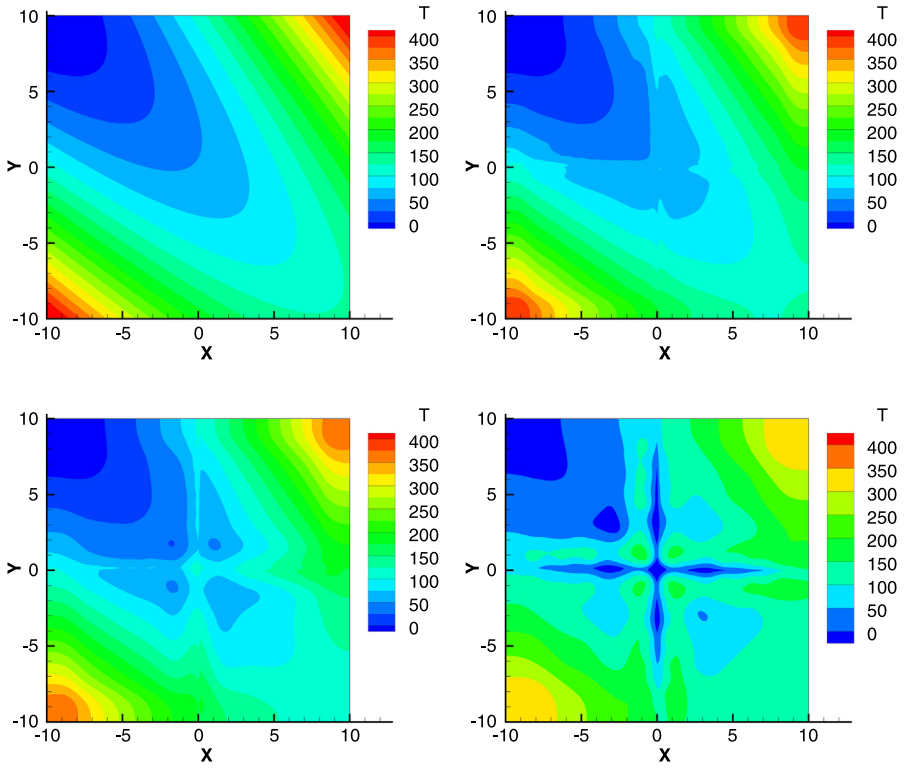

Fig. 8. Example 2: The comparison of the exact source function (top left) with the reconstructed source function with the measurement data ratio $r = \frac{1}{6}$ (top right), $\frac{1}{8}$ (bottom left), $\frac{1}{12}$ (bottom right).

Table 3
The comparison with different boundary conditions on Γ_i'.

		Ex1		Ex2		Ex3	
θ	ϵ	E_0	E_ϵ	E_0	E_ϵ	E_0	E_ϵ
0.1	1%	4.3598	0.0515	3.1285	0.0256	5.4872	0.0648
	3%	4.4286	0.1168	3.1770	0.0320	5.5728	0.0913
	5%	4.4985	0.1616	3.2255	0.0445	5.6586	0.1234
	10%	4.6777	0.2287	3.3472	0.0832	5.8745	0.2096
0.2	1%	0.6440	0.0389	0.4561	0.0135	0.8185	0.0574
	3%	0.6664	0.0799	0.4677	0.0251	0.8395	0.0830
	5%	0.6944	0.1205	0.4799	0.0366	0.8621	0.1037
	10%	0.7847	0.1978	0.5125	0.0744	0.9249	0.1676
0.3	1%	0.1480	0.0372	0.0998	0.0131	0.1919	0.0590
	3%	0.1722	0.0727	0.1026	0.0244	0.1997	0.0819
	5%	0.2101	0.1005	0.1079	0.0391	0.2133	0.1038
	10%	0.3309	0.1752	0.1304	0.0694	0.2658	0.1428
0.4	1%	0.0670	0.0365	0.0404	0.0153	0.0973	0.0643
	3%	0.1032	0.0748	0.0440	0.0254	0.1080	0.0825
	5%	0.1493	0.1014	0.0531	0.0395	0.1269	0.1051
	10%	0.2745	0.1729	0.0867	0.0698	0.1924	0.1434
0.5	1%	0.0558	0.0368	0.0353	0.0165	0.0903	0.0661
	3%	0.0814	0.0731	0.0398	0.0259	0.1024	0.0826
	5%	0.1141	0.1039	0.0463	0.0398	0.1140	0.1045
	10%	0.2038	0.1728	0.0774	0.0732	0.1607	0.1460

4.5. Parallel performance

In this experiment we study the parallel performance of the proposed algorithm with different domain decompositions. Recall that m_1 and m_2 denote the number of the subdomains at the first and the second level respectively. We consider

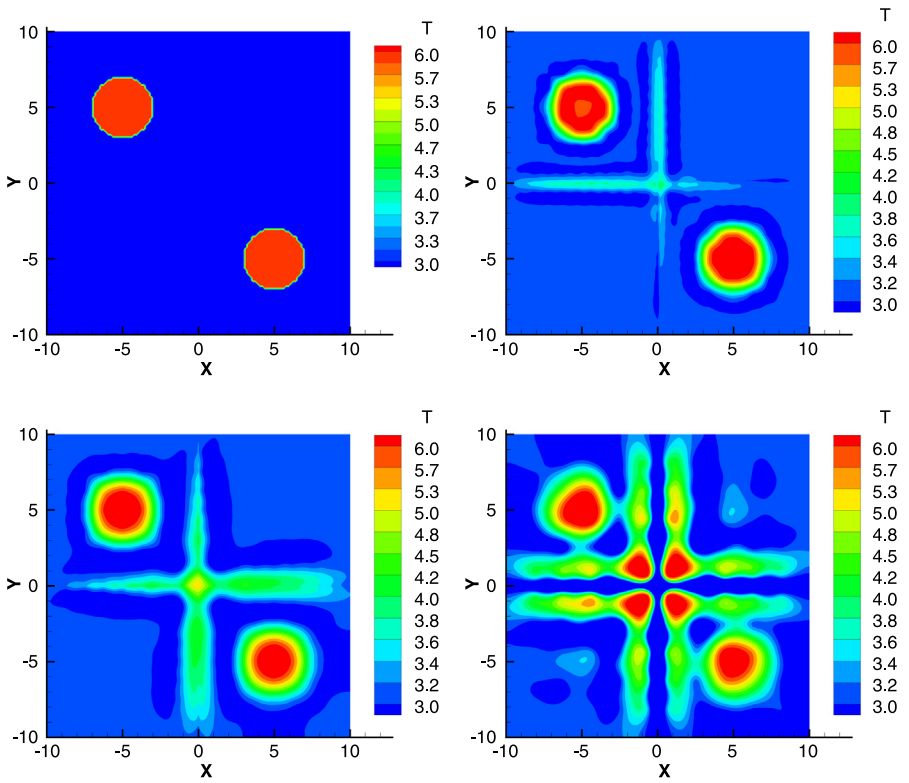

Fig. 9. Example 3: The comparison of the exact source function (top left) with the reconstructed source function with the measurement data ratio $r = \frac{1}{6}$ (top right), $\frac{1}{8}$ (bottom left), $\frac{1}{12}$ (bottom right).

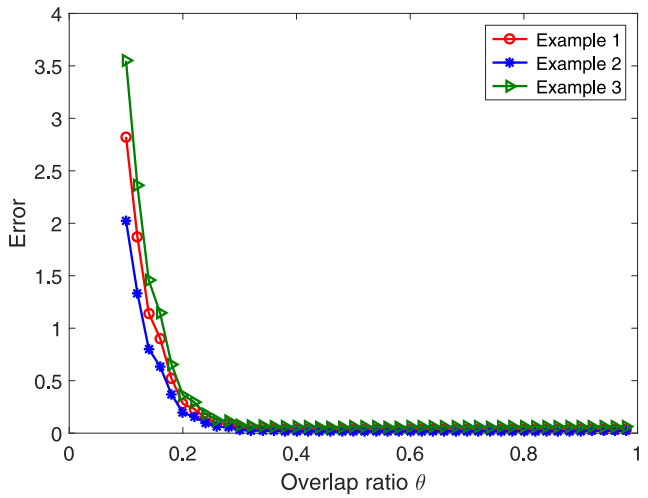

Fig. 10. The plot of reconstruction error with respect to the overlap ratio for Examples 1 (red circle), 2 (blue star) and 3 (green triangle).

eight combinations of m_1 and m_2 as follows: $\{(m_1, m_2)\} = \{(1, 1296), (4, 324), (9, 144), (16, 81), (36, 36), (144, 9), (324, 4), (1296, 1)\}$. $np = 1296$ processors are used for the experiment since $m_1 \times m_2 = 1296$. We use a larger computational domain $\Omega = [-100, 100] \times [-100, 100]$ than the previous experiments and the overlap ratio is $\theta = 0.5$. The measurement data is obtained by solving the problem on a 4801×4801 mesh. The level of noise is chosen as $\epsilon = 1\%$. For comparison, we ensure almost the same problem size and the same mesh size to compute the inverse problem for the eight choices of m_1 and m_2. The mesh for $m_1 = 1$ is 2401×2401, which is the case of classical method with domain decomposition only for the RAS preconditioner, and the meshes on the subdomains Ω_i' are 1201×1201, 801×801,

Table 4
The parallel performance with $np = 1296$ and two types of boundary conditions.

Ex1		Homogeneous BC				Measurement data BC			
m_1	m_2	*its*	Time (s)	E_0	S	*its*	Time (s)	E_ϵ	S
1	1296	231	3.2949	0.0709	1	231	3.2949	0.0709	1
4	324	112	1.4660	0.0540	2.25	118	1.3304	0.0540	2.48
9	144	83	0.9224	0.0538	3.57	85	0.8346	0.0538	3.95
16	81	73	0.7676	0.0538	4.29	58	0.6400	0.0561	5.15
36	36	28	0.3010	0.0765	10.95	28	0.3041	0.0780	10.83
144	9	26	0.2513	0.0799	13.11	25	0.2464	0.0751	13.37
324	4	23	0.2016	0.0839	16.34	24	0.2057	0.0828	16.02
1296	1	21	0.1739	3.071	18.95	22	0.1775	0.0867	18.56
Ex2		Homogeneous BC				Measurement data BC			
m_1	m_2	*its*	Time (s)	E_0	S	*its*	Time (s)	E_ϵ	S
1	1296	226	2.5858	0.0095	1	226	2.5858	0.0095	1
4	324	112	1.6477	0.0156	1.57	112	1.3742	0.0123	1.88
9	144	84	0.9234	0.0155	2.80	83	0.8931	0.0143	2.90
16	81	31	0.3553	0.0165	7.28	32	0.3612	0.0174	7.16
36	36	28	0.2968	0.0174	8.71	28	0.2963	0.0162	8.73
144	9	24	0.2428	0.0137	10.65	24	0.2418	0.0183	10.69
324	4	23	0.2047	0.0824	12.63	23	0.2052	0.0211	12.60
1296	1	22	0.1668	17.916	15.50	22	0.1768	0.0357	14.63
Ex3		Homogeneous BC				Measurement data BC			
m_1	m_2	*its*	Time (s)	E_0	S	*its*	Time (s)	E_ϵ	S
1	1296	222	3.2636	0.0168	1	222	3.2636	0.0168	1
4	324	111	1.2806	0.0312	2.55	111	1.5783	0.0296	2.07
9	144	84	0.8901	0.0279	3.67	84	0.8819	0.0273	3.70
16	81	56	0.6193	0.0312	5.27	57	0.6243	0.0299	5.23
36	36	28	0.3050	0.0314	10.70	28	0.2978	0.0280	10.96
144	9	24	0.2440	0.0252	13.38	25	0.2477	0.0346	13.18
324	4	23	0.2028	0.1471	16.09	23	0.2045	0.0374	15.96
1296	1	21	0.1757	31.5620	18.57	22	0.1759	0.0607	18.55

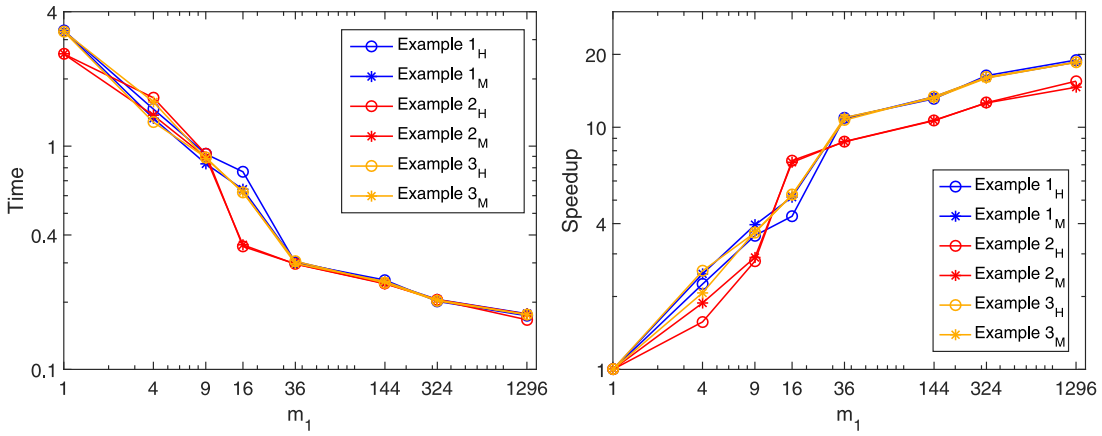

Fig. 11. The computing time and the speedup of Examples 1–3. Left: computing time, right: speedup.

601×601, 401×401, 201×201, 133×133, and 67×67 respectively for $m_1 = 4, 9, 16, 36, 144, 324, 1296$. The measurements ratio is chosen as $r = \frac{1}{4}$.

The average number of GMRES iterations, the average computing time, the reconstruction error and the speedup, denoted by S, are shown in Table 4 for both homogeneous boundary conditions (Columns 3–6) and measurement data boundary conditions (Columns 7–10) on Γ_i' respectively. It is noted that the speedup S is defined as the ratio of the computing time using $m_1 > 1$ subdomains and the computing time obtained with $m_1 = 1$. We also plot the average computing time (Columns 4,8) and the speedup (Columns 6,10) in Fig. 11, where the results computed with homogeneous and measurement data boundary conditions are denoted by "Example i_H" and "Example i_M" respectively, $i = 1, 2, 3$. It is observed from the speedup that the parallel performance is much improved when the partition happens at the optimization level; i.e., $m_1 > 1$, compared with the case of $m_1 = 1$. For Examples 1 and 3, when $m_1 \leq 36$, with increasing

number of subdomains m_1 at the first level, the average number of GMRES iterations and the computing time decrease almost linearly with m_1. The reconstruction errors are quite satisfactory and increase very slowly with m_1. The parallel performance and the reconstruction error for both types of boundary conditions are similar. However when $m_1 > 36$, we observe a small decrease in the average number of GMRES iterations and in the computing time despite increasing m_1 for both type of boundary conditions. The reconstruction errors for homogeneous boundary conditions (Column 5) increase faster than that for measurement data boundary conditions (Column 9), especially for $m_1 = 1296$, which means one processor per subproblem without the second level of domain decomposition, the reconstruction error blows up for using homogeneous boundary conditions and stays quite reasonable for using measurement data boundary conditions. Similar phenomena are observed for Example 2 when $m_1 = 16$.

5. Some final remarks

We propose and test a multilevel domain decomposition method for the 2D steady source identification problem governed by elliptic equations. The domain is decomposed firstly into several subdomains to transform the original optimization formulation of the inverse problem into smaller independent optimization problems defined on overlapping subdomains. Each sub-optimization problem is then converted to a KKT system of equations that is solved by a restarted GMRES method preconditioned by a restricted additive Schwarz preconditioner. When forming the preconditioner, a second level of domain decomposition is introduced for each first-level subdomain. We provide a theoretical analysis to show that these sub-optimization problems are solvable, the numerical solution is well-posed and the error of the reconstructed solution is bounded by a constant depending on the noise level, the number of subdomains and the error from the inexact boundary conditions. Two types of conditions on the artificial boundaries are investigated and we conclude that, the parallel performances are similar, but the solution error using measurement data is smaller compared with using homogeneous boundary conditions when the overlap is small. Numerical experiments also show that the accuracy of the proposed algorithm is similar with the classical approach without any decomposition at the optimization level, and the new method offers much better parallel performance. The algorithm is not designed specifically for the source identification problem, it should be useful for other large scale inverse parameter identification problems. Our next work is to extend this method for the more complex three-dimensional problems.

Acknowledgment

The work of the first two authors was supported by the Natural Science Foundation of Guangdong Province, China (Projects 2020A1515010704 and 2114050000592).

Appendix

We here provide a proof of Lemma 3.1.

Proof of Lemma 3.1. Let $a(u,\phi) = (a\nabla u, \nabla\phi) = \int_\Omega a(\mathbf{x})\nabla u\cdot\nabla\phi dx$, $(f,\phi) = \int_\Omega f\phi dx$, clearly $a(\cdot,\cdot)$ is a symmetric bilinear form. Since $p(x) \in H^{\frac{1}{2}}(\partial\Omega)$, by the trace theorem (cf. [35] Theorem 3.38, page 102), we can find a function $u_p \in H^1(\Omega)$, such that $\gamma u_p = p(x)$ with γ being the trace operator. Let $w = u - u_p$, then w is the solution of the following PDE:

$$\begin{cases} -\nabla\cdot(a\nabla w) = f + \nabla\cdot(a\nabla u_p), & \mathbf{x}\in\Omega \\ w = 0, & \mathbf{x}\in\partial\Omega. \end{cases} \tag{A.1}$$

The weak formulation of (A.1) is equivalent to find $w \in H_0^1(\Omega)$, such that

$$a(w,\eta) = (f,\eta) - a(u_p,\eta), \quad \forall\eta\in H_0^1(\Omega).$$

By the Poincaré's inequality,

$$a(w,w) = (a(x)\nabla w, \nabla w) \geq a_1\int_\Omega |\nabla w|^2 dx \geq Ca_1\|w\|_{1,\Omega}^2,$$

$a(\cdot,\cdot)$ is coercive in $H_0^1(\Omega)$. And $a(\cdot,\cdot)$ is continuous in $H_0^1(\Omega)$ by the Cauchy–Schwarz inequality,

$$a(w,\eta) = (a(x)\nabla w, \nabla\eta) \leq a_2|w|_{1,\Omega}|\eta|_{1,\Omega} \leq a_2\|w\|_{1,\Omega}\|\eta\|_{1,\Omega}.$$

By the Lax–Milgram theorem, there exists a unique solution w, and we have the following estimates

$$\begin{aligned} a_1\|w\|_{1,\Omega}\|\eta\|_{1,\Omega} &\leq Ca(w,\eta) = C((f,\eta) - a(u_p,\eta)) \\ \|w\|_{1,\Omega} &\leq \frac{C}{a_1}(\|f\|_{-1,\Omega} + a_2\|u_p\|_{1,\Omega}). \end{aligned}$$

Since $w = u - u_p$, $\|w\|_{1,\Omega} \geq \|u\|_{1,\Omega} - \|u_p\|_{1,\Omega}$, we have

$$\|u\|_{1,\Omega} \leq \frac{C}{a_1}\|f\|_{-1,\Omega} + \left(\frac{Ca_2}{a_1} + 1\right)\|u_p\|_{1,\Omega}$$

$$\|u\|_{1,\Omega} \leq \frac{C}{a_1}\|f\|_{-1,\Omega} + \left(\frac{Ca_2}{a_1} + 1\right)\inf_{u\in H^1(\Omega),\gamma u=p}\|u\|_{1,\Omega}$$

$$\|u\|_{1,\Omega} \leq \frac{C}{a_1}\|f\|_{-1,\Omega} + \left(\frac{Ca_2}{a_1} + 1\right)\|p\|_{\frac{1}{2},\partial\Omega}.$$

References

[1] A.E. Badia, T. Ha-Duong, An inverse source problem in potential analysis, Inverse Problems 16 (2000) 651–663, http://dx.doi.org/10.1088/0266-5611/16/3/308.

[2] A.E. Badia, A.E. Hajj, M. Jazar, H. Moustafa, Identification of point sources in an elliptic equation from interior measurements: Application to a seawater intrusion problem, J. Inverse Ill-Posed Probl. 27 (4) (2019) 559–574, http://dx.doi.org/10.1515/jiip-2018-0095.

[3] M. Anastasio, J. Zhang, D. Modgil, P. Rivière, Application of inverse source concepts to photoacoustic tomography, Inverse Problems 23 (2007) S21–S35, http://dx.doi.org/10.1088/0266-5611/23/6/S03.

[4] V. Akçelik, G. Biros, O. Ghattas, K.R. Long, B. Waanders, A variational finite element method for source inversion for convective-diffusive transport, Finite Elem. Anal. Des. 39 (2003) 683–705, http://dx.doi.org/10.1016/s0168-874x(03)00054-4.

[5] G. Biros, G. Dogan, A multilevel algorithm for inverse problems with elliptic PDE constraints, Inverse Problems 24 (3) (2008) 034010, http://dx.doi.org/10.1088/0266-5611/24/3/034010.

[6] S.S. Adavani, G. Biros, Fast algorithms for source identification problems with elliptic PDE constraints, SIAM J. Imaging Sci. 3 (4) (2010) 791–808, http://dx.doi.org/10.1137/080738064.

[7] Y.C. Hon, M. Li, Y.A. Melnikov, Inverse source identification by Green's function, Eng. Anal. Bound. Elem. 34 (2010) 352–358, http://dx.doi.org/10.1016/j.enganabound.2009.09.009.

[8] M. Hanke, W. Rundell, On rational approximation methods for inverse source problems, Inverse Probl. Imaging 5 (1) (2011) 185–202, http://dx.doi.org/10.3934/ipi.2011.5.185.

[9] A. Hamad, M. Tadi, A numerical method for inverse source problems for Poisson and Helmholtz equations, Phys. Lett. A 380 (44) (2016) 3707–3716, http://dx.doi.org/10.1016/j.physleta.2016.08.057.

[10] J.-C. Liu, An inverse source problem of the Poisson equation with Cauchy data, Electron. J. Differential Equations 119 (2017) 1–19.

[11] M.-E. Amin, X. Xiong, Source identification problems for radially symmetric and axis-symmetric heat conduction equations, Appl. Numer. Math. 138 (2019) 1–18, http://dx.doi.org/10.1016/j.apnum.2018.12.013.

[12] T.-T. Binh, H.-K. Nashine, N.-H. Luc, C. Nguyen, Identification of source term for the ill-posed Rayleigh-Stokes problem by Tikhonov regularization method, Adv. Differential Equations 2019 (331) (2019) 1–20, http://dx.doi.org/10.1186/s13662-019-2261-7.

[13] J. Kang, L. Kallivokas, The inverse medium problem in 1D PML-truncated heterogeneous semi-infinite domains, Inverse Probl. Sci. Eng. 18 (6) (2010) 759–786, http://dx.doi.org/10.1080/17415977.2010.492510.

[14] X.-C. Cai, S. Liu, J. Zou, Parallel overlapping domain decomposition methods for coupled inverse elliptic problems, Commun. Appl. Math. Comput. Sci. 4 (2009) 1–26, http://dx.doi.org/10.2140/camcos.2009.4.1.

[15] X. Deng, X.-C. Cai, J. Zou, A parallel space-time domain decomposition method for unsteady source inversion problems, Inverse Probl. Imaging 9 (2015) 1069–1091, http://dx.doi.org/10.3934/ipi.2015.9.1069.

[16] S. Takacs, A robust all-at-once multigrid method for the Stokes control problem, Numer. Math. 130 (3) (2015) 517–540, http://dx.doi.org/10.1007/s00211-014-0674-5.

[17] Y. Saad, Iterative Methods for Sparse Linear Systems, second ed., SIAM, 2003, http://dx.doi.org/10.1137/1.9780898718003.

[18] L. Luo, L. Liu, X.-C. Cai, D.-E. Keyes, Fully implicit hybrid two-level domain decomposition algorithms for two-phase flows in porous media on 3D unstructured grids, J. Comput. Phys. 409 (2020) 109312, http://dx.doi.org/10.1016/j.jcp.2020.109312.

[19] Z.-J. Liao, R. Chen, Z. Yan, X.-C. Cai, A parallel implicit domain decomposition algorithm for the large eddy simulation of incompressible turbulent flows on 3D unstructured meshes, Internat. J. Numer. Methods Fluids 89 (9) (2019) 343–361, http://dx.doi.org/10.1002/fld.4695.

[20] F. Kong, Neutron transport criticality calculations using a parallel monolithic multilevel Schwarz preconditioner together with a nonlinear diffusion acceleration method, Ann. Nucl. Energy 141 (2020) 107342, http://dx.doi.org/10.1016/j.anucene.2020.107342.

[21] B. Smith, P. Bjørstad, W. Gropp, Domain Decomposition: Parallel Multilevel Methods for Elliptic Partial Differential Equations, Cambridge University Press, 2004.

[22] X. Deng, X.-C. Cai, J. Zou, Two-level space-time domain decomposition methods for three-dimensional unsteady inverse source problems, J. Sci. Comput. 67 (2016) 860–882, http://dx.doi.org/10.1007/s10915-015-0109-1.

[23] P. Antonietti, P. Houston, G. Pennesi, E. Süli, An agglomeration-based massively parallel non-overlapping additive Schwarz preconditioner for high-order discontinuous Galerkin methods on polytopic grids, Math. Comp. 89 (2020) 2047–2083, http://dx.doi.org/10.1090/mcom/3510.

[24] S.-R. Cai, J.-Y. Xiao, Y.-C. Tseng, F.-N. Hwang, Parallel smoothed aggregation multilevel schwarz preconditioned Newton-Krylov algorithms for Poisson-Boltzmann problems, Numer. Math. Theory Methods 13 (3) (2020) 745–769, http://dx.doi.org/10.4208/nmtma.OA-2019-0174.

[25] J. Wang, E. Chung, H.-H. Kim, A two-level overlapping Schwarz method with energy-minimizing multiscale coarse basis functions, J. Comput. Appl. Math. 370 (2020) 112600, http://dx.doi.org/10.1016/j.cam.2019.112600.

[26] R. Chen, J. Huang, X.-C. Cai, A parallel domain decomposition algorithm for large scale image denoising, Inverse Probl. Imaging 13 (6) (2019) 1259–1282, http://dx.doi.org/10.3934/ipi.2019055.

[27] M.-C. Lai, Y.-H. Tseng, A fast iterative solver for the variable coefficient diffusion equation on a disk, J. Comput. Phys. 208 (2005) 196–205, http://dx.doi.org/10.1016/j.jcp.2005.02.005.

[28] H. Ji, F.-S. Lien, E. Yee, An efficient second-order accurate cut-cell method for solving the variable coefficient Poisson equation with jump conditions on irregular domains, Internat. J. Numer. Methods Fluids 52 (7) (2006) 723–748, http://dx.doi.org/10.1002/fld.1199.

[29] A. Raeli, M. Bergmann, A. Lollo, A finite-difference method for the variable coefficient Poisson equation on hierarchical Cartesian meshes, J. Comput. Phys. 355 (2018) 59–77, http://dx.doi.org/10.1016/j.jcp.2017.11.007.

[30] Y. Liu, Y. He, Two-level Schwarz methods for a discontinuous Galerkin approximation of elliptic problems with jump coefficients, J. Sci. Comput. 84 (1) (2020) 1–33, http://dx.doi.org/10.1007/s10915-020-01257-2.

[31] H.W. Engl, M. Hanke, A. Neubauer, Regularization of Inverse Problems, Kluwer Academic Publishers, Netherland, 1996, http://dx.doi.org/10.1007/978-94-009-1740-8.

[32] X.-C. Cai, M. Sarkis, A restricted additive Schwarz preconditioner for general sparse linear systems, SIAM J. Sci. Comput. 21 (1999) 792–797, http://dx.doi.org/10.1137/S106482759732678X.
[33] L.C. Evans, Partial Differential Equations, second ed., American Mathematical Society, 2010, http://dx.doi.org/10.1090/gsm/019.
[34] S.E. Mikhailov, Traces, extensions and co-normal derivatives for elliptic systems on Lipschitz domains, J. Math. Anal. Appl. 378 (2011) 324–342, http://dx.doi.org/10.1016/j.jmaa.2010.12.027.
[35] W. McLean, Strongly Elliptic Systems and Boundary Integral Equations, Cambridge University Press, 2000.
[36] W. Rudin, Functional Analysis, second ed., McGraw-Hill, Inc., 1991.